FlatChem 17 (2019) 100130

Contents lists available at ScienceDirect

FlatChem

journal homepage: www.elsevier.com/locate/flatc

ALD growth of MoS_2 nanosheets on TiO_2 nanotube supports

Hanna Sopha[a,b], Alexander T. Tesfaye[c], Raul Zazpe[a,b], Jan Michalicka[b], Filip Dvorak[a], Ludek Hromadko[a,b], Milos Krbal[a], Jan Prikryl[a], Thierry Djenizian[c], Jan M. Macak[a,b,*]

[a] Center of Materials and Nanotechnologies, Faculty of Chemical Technology, University of Pardubice, Nam. Cs. Legii 565, 53002 Pardubice, Czech Republic
[b] Central European Institute of Technology, Brno University of Technology, Purkyňova 123, 612 00 Brno, Czech Republic
[c] Mines Saint-Etienne, Center of Microelectronics in Provence, Flexible Electronics Department, 13541 Gardanne, France

ARTICLE INFO

Keywords:
TiO_2 nanotube layers
MoS_2 nanosheets
Atomic layer deposition
Li-ion microbatteries

ABSTRACT

Two-dimensional MoS_2 nanostructures are highly interesting and effective in a number of energy-related applications. In this work, the synthesis of ultra-thin MoS_2 nanosheets produced by the thermal Atomic Layer Deposition (ALD) process is reported for the first time using a previously unpublished set of precursors, namely bis(t-butylimido)bis(dimethylamino)molybdenum and hydrogen sulfide. These nanosheets are homogenously deposited within one-dimensional anodic TiO_2 nanotube layers that act as a high surface area conductive support for the MoS_2 nanosheets. The decoration of high aspect ratio TiO_2 nanotube layers with MoS_2 nanosheets over the entire nanotube layer thickness is shown for the first time. The homogeneous distribution of the MoS_2 nanosheets is proved by STEM/EDX. This resulting new composite is employed as anode for Li-ion microbatteries. The MoS_2-decorated TiO_2 nanotube layers show a superior performance compared to their counterparts without MoS_2. Compared to electrochemical performance of pristine TiO_2 nanotube, a more than 50% higher areal capacity and a coulombic efficiency of 98% are obtained on the MoS_2 decorated TiO_2 nanotube layers, demonstrating clear synergic benefits of the new composite structure.

1. Introduction

In the last 15 years, anodic self-organized TiO_2 nanotube (TNT) layers have attracted considerable interest motivated by their wide range of applications, such as solar cells, sensors or batteries [1–3]. The advantage of TNT layers compared to other nanostructures, e.g. nanoparticles or fibers, is their high self-ordering degree and the straight vertical alignment on the Ti substrate and in general a very high available surface area. Meanwhile, the anodic TNT layers can be produced with distinct dimensions, i.e. nanotube diameter and layer thickness, using well-established anodization protocols [1,3]. To improve their performance and increase the range of functionality for different applications TNT layers are often decorated [4], filled [5,6] or coated [7,8] with secondary materials. Such modifications can lead for instance to a shift of light absorption from UV to VIS light [7] or to an improved stability and performance in batteries [8]. These modifications can be carried out by a variety of different methods, such as electrodeposition [5,6], sputtering [9,10], chemical bath decoration [11,12], spincoating [13,14], vapor deposition [15], etc. However, all these methods suffer from inhomogeneous coating of high aspect ratio TNT layers. Recently, Atomic Layer Deposition (ALD) was introduced as a technique being able to uniformly coat even extremely high aspect ratio TNT layers with controllable coating composition and thickness [7,16–18].

MoS_2, a transition metal dichalcogenide (TMDC) featuring a two-dimensional covalently bonded triplet layered S-Mo-S structure (graphene-like) that is held together along the third dimension by weak van-der-Waals forces [19,20], is well-known as an electrocatalyst for hydrogen evolution reaction [21,22]. However, it is an interesting anode material for lithium ion microbatteries (μLIBs). The weak interlayer interaction of MoS_2 allows Li^+ to intercalate between the layers without a significant volumetric expansion [23,24]. The first report on the Li^+ intercalation into MoS_2 dates back to 1959 [25]. However, as the bulk MoS_2 does not offer exciting electrochemical properties for lithium storage, the application has not been very successful. In the recent years, huge attention has been focused on nanostructured MoS_2 [26]. The MoS_2 nanostructures, such as nanoflakes [27], nanosheets [28–34], nanobelts [35], or MoS_2 nano-composites [36,37], are mainly prepared via hydrothermal synthesis [28–30,32,34,35] and have to be mixed with a conducting agent and a binder to be fixed on a copper foil

* Corresponding author at: Center of Materials and Nanotechnologies, Faculty of Chemical Technology, University of Pardubice, Nam. Cs. Legii 565, 53002 Pardubice, Czech Republic.
E-mail address: jan.macak@upce.cz (J.M. Macak).

https://doi.org/10.1016/j.flatc.2019.100130
Received 28 May 2019; Received in revised form 28 June 2019; Accepted 12 July 2019
Available online 02 August 2019

to be used as electrode for Li-ion batteries (LIBs). Alternatively, MoS_2 nanosheets, grown via ALD on conductive substrates [38–47], can be used as binder free anodes in LIBs [38,39]. However, in these two reports [38,39] relatively thick ALD MoS_2 layers were used, i.e. 40 nm and 70 nm, respectively, while some recent reports [29,31] show that already few-layered MoS_2 nanosheets can show good performances in LIBs. Few-layered MoS_2 nanosheets, with many active side edges (electrochemically active) [21,48–50], deposited on large surface area substrates, such as TNT layers, could, therefore, be excellent anodes in μLIBs.

Anodic TNT layers have been decorated and coated with MoS_2 by different techniques, such as via photocatalytic reduction of $(NH_4)_2MoS_4$ into MoS_2 nanoparticles [51], electrodeposition [52,53], hydrothermal routes [54,55], sputtering [10], or physical and chemical vapor deposition [15]. However, all these reports use either relatively thin, low aspect-ratio TNT layers, i.e. with thicknesses below 1 μm [15,51,53], or show incomplete coating of higher aspect ratio TNT layers [10,52,54,55]. Furthermore, the coated or decorated TNT layers were only employed for (photo-)catalysis [10,15,51–53,55] or for alcohol sensing [54]. Only one report can be found in the literature on the use of a TNT@carbon@MoS_2 heterostructure in LIBs [56]. However, in this report several days were needed to produce the modified TNTs via a multi-step synthesis. Another disadvantage of this procedure is the fact that the obtained TNTs are not ordered and have to be deposited with a binder on a Cu foil.

In this paper, for the first time the homogenous decoration of high aspect-ratio anodic TNT layers with ultra-thin MoS_2 nanosheets using ALD is reported. For this, a new combination of a non-halide Mo precursor (i.e. to avoid the use of $MoCl_5$, which corrodes the ALD tool) and H_2S, which can be used at low temperatures and has no detrimental effect on the TNT layers during the ALD process and on the ALD tool itself, was used. The homogeneous decoration of the TNT layers over their entire thickness and available surface area is shown using STEM/EDX, and the composition of the MoS_2 nanosheets is evaluated by XPS. It is also shown that the MoS_2-decorated TNT layers are promising materials as negative electrodes for μLIBs. They show a superior electrochemical performance in comparison to their pristine counterparts. The state of art in the utilization of the TiO_2-MoS_2 nanostructures for Li-ion batteries is significantly moved forward.

2. Material and methods

Self-organized TiO_2 nanotube layers (TNTs) with a thickness of ~20 μm and a diameter of ~110 nm (yielding an aspect ratio of ~180) were produced by electrochemical anodization of thin Ti foils (Sigma-Aldrich, 127 μm thick, 99.7% purity) according to the previously published work [57]. In brief, prior to anodization the Ti foils were degreased by sonication in isopropanol and acetone and dried in air. The anodization was carried out at 60 V for 4 h in an ethylene glycol based electrolyte containing 170 mM NH_4F and 1.5 vol% H_2O. The electrochemical cell consisted of a high voltage potentiostat (PGU-200 V; Elektroniklabor GmbH) in a two-electrode configuration, with a Pt foil as counter electrode and the Ti foil as working electrode. After anodization, the nanotube layers were sonicated in isopropanol and dried in air. Before further use, the TNTs were annealed in a muffle oven at 400 °C for 1 h to receive crystalline anatase phase.

The deposition of MoS_2 within TNTs was carried out via ALD (Beneq TFS-200). Bis(t-butylimido)bis(dimethylamino)molybdenum (Strem, 98%) and hydrogen sulfide (99.5%) were used as molybdenum and sulphur precursors, respectively. The MoS_2 was deposited within the nanotube layers by applying different numbers of ALD cycles: 2, 60 and 225 cycles. All processes were carried out at a temperature of 275 °C, and using N_2 (99.9999%) as carrier gas at a flow rate of 500 standard cubic centimeters per minute (sccm). The molybdenum precursor was heated up to 75 °C to increase its vapour pressure. Under these deposition conditions, one growth ALD cycle was defined by the following sequence: Bis(t-butylimido)bis(dimethylamino) molybdenum pulse (4 s) - Bis(t-butylimido)bis(dimethylamino) molybdenum exposure (45 s) - N_2 purge (90 s) - H_2S pulse (2.5 s) - H_2S exposure (45 s) - N_2 purge (90 s). The combination of the used precursors has not been found so far in the literature for thermal ALD (see Table S1) and it is an interesting option to the $MoCl_5$-H_2S process [41].

Cyclic voltammograms in an aqueous 0.1 M Na_2SO_4 solutions were recorded in dark to compare intrinsic electronic conductivities of the anodes using modular electrochemical system AUTOLAB (PGSTAT 204, Metrohm Autolab B.V., *Nova 1.10* software) in a three-electrode set-up, with Ag/AgCl reference electrode, a Pt wire as counter electrode, and the TNT layers as working electrode.

The electrochemical performance tests were performed using standard two-electrode Swagelok cells that were assembled in a glovebox filled with high purity argon (Ar). The half-cells were consisted of MoS_2 decorated TNTs as the working electrode and Li foil as the reference electrode. The two electrodes were separated by a Whatman glass microfiber soaked in organic liquid electrolyte solution composed of 1 M $LiPF_6$ dissolved in a 1:1 w/w mixture of ethylene carbonate (EC) and dimethyl carbonate (DMC).

The electrochemical performance tests (cyclic voltammetry (CV) and galvanostatic charge–discharge) were performed using a VMP3 potentiostat (Bio Logic, France). The CV curves were recorded in a potential window of 0.01–3 V at a scan rate of 0.5 mV s^{-1}. Galvanostatic tests were performed at 1C in the potential window of 0.01–3 V. C/n means the battery is fully charged or discharged up to its total storage capacity in *n* hours. In line with the literature on the Li-ion microbatteries [58,59], areal capacities were used, instead of the gravimetric capacities. The surface area of the both blank and MoS_2-decorated TNT layers was considered as a macroscopic surface area (0.79 cm^2) used for the microbattery with a diameter of the active area of 1 cm.

The structure and morphology of the pristine and MoS_2-decorated TNTs were characterized by field-emission scanning electron microscope (FE-SEM JEOL JSM 7500F) and a high-resolution transmission electron microscope (FEI Titan Themis 60–300, operated at 60 keV) equipped with a high angle annular dark field detector for scanning transmission electron microscopy (HAADF-STEM) and SUPER-X energy dispersive X-ray (EDX) spectrometer with 4 × 30 mm^2 windowless silicon drift detectors. All the presented EDX maps are shown in atomic % calculated from measured intensities by k-factor method implemented in used software Velox 2.5. Cross section views were obtained from mechanical bended TNTs.

The X-ray diffraction (XRD) patterns were measured on Panalytical Empyrean diffractometer using a Cu X-ray tube and a scintilation detector Pixcel^{3D}. The measurement were performed in the 2θ range of 5–65°, the step size was 0.026°. The diffractometer was equipped with a *xyz* programmable stage, which allows to adjust height and position of the sample.

The composition of MoS_2 was monitored by X-ray photoelectron spectroscopy (XPS) (ESCA2SR, Scienta-Omicron) using a monochromatic Al Kα (1486.7 eV) X-ray source. The binding energy scale was referenced to adventitious carbon (284.8 eV). The quantitative analysis was performed using the elemental sensitivity factors provided by the manufacturer.

3. Results and discussion

3.1. Characterization of ALD MoS_2-decorated TNTs

Fig. 1a and b show SEM images of the as-prepared anodic TNT layers. Obviously, the TNTs are highly ordered, closed packed and possess an internal diameter of ~110 nm. The thickness of the TNT layers was ~20 μm, giving an aspect ratio of ~180. It was not possible to observe the MoS_2 nanosheets on the MoS_2-decorated TNTs, due to their extremely small thickness (heights), since only 2 MoS_2 ALD cycles

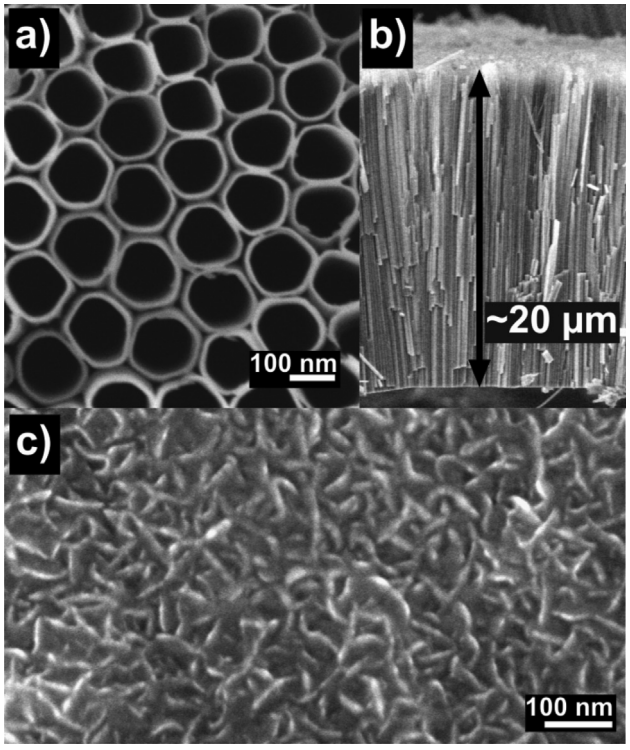

Fig. 1. SEM images of the as-prepared TNT layers: (a) top view, (b) cross-section and (c) SEM image of MoS_2 sheets on a flat Ti foil produced by 225 ALD cycles of the MoS_2 process.

were used herein. Nevertheless, when a considerably larger number of ALD cycles was used, it was possible to visualize larger MoS_2 nanosheets. Fig. 1c shows a representative SEM image of a reference Ti foil for which 225 ALD cycles of the MoS_2 process were used. The nature of the ALD grown MoS_2 nanosheets is clearly observed, which fits to the typical morphology of this material (and other TMDCs), produced by various techniques [50,60]. Due to the extremely small size of the MoS_2 nanosheets, scanning transmission electron microscopy (STEM) along with energy dispersive X-ray spectroscopy (EDX) was used to characterize the nanosheets in more details. Fig. 2a shows the STEM/EDX elemental maps of the chemical distribution of Mo and S elements on fragments of two adjacent TiO_2 nanotubes in the cross-sectional view. These maps reveal that MoS_2 was deposited within the TNT walls after 2 ALD cycles. However, individual MoS_2 nanosheets could not be revealed by atomic high resolution imaging in STEM or TEM mode due to too thick TNT walls. However, a detailed view on the EDX maps in Fig. 2a reveals a MoS_2 decoration at the edges of the TNT walls. Given the number of ALD cycles used in this work (i.e. 2 cycles), the principle of the ALD growth and the layered nature of 2D materials (including MoS_2 [50]), the individual MoS_2 nanosheets consist of 1–2 MoS_2 layers at maximum. Given also the nanoscale dimensions of the TNT wall - MoS_2 nanosheet interface and the high magnification during the STEM imaging (to be judged from the scale bar), the nanosheets are very likely thinner than 1 nm. Based on the TMDCs literature evidence, MoS_2 follows the Volmer-Weber growth mode, which can be attributed to a dominant atom-to-atom interaction. This was studied and discussed in detail for PbTe and PbSe [61]. Thus, during the initial ALD cycles an island growth was observed, while for higher cycle numbers a homogenous MoS_2 film consisting of MoS_2 nanosheets was found (see Fig. 1c for comparison with the MoS_2 ALD 225 cycle case). This phenomenon can also be found in the literature for ALD MoS_2 produced with other precursors [41,62].

Fig. 2b shows a high angle annular dark field (HAADF) STEM image of a fragment of a TNT in the planar view and corresponding EDX maps. These data reveal the presence of numerous Mo- and S-rich nanosheets on the TNT walls, with rather irregular shape and a width of about 10–15 nm. By detailed inspection of the decorated TNTs, a homogenous and uniform decoration of the TNT layers with MoS_2 nanosheets was revealed over their entire volume. These results are in good accordance with the previous studies of coating or decoration of 20 µm long TNT layers with secondary materials using ALD [57,63,64].

To obtain additional information on the crystalline structure and composition of the MoS_2 nanosheets, XRD and XPS analyses were carried out. Fig. 3 shows the XRD patterns of the TNT layer decorated with 2 MoS_2 ALD cycles over the 2θ range from 10° to 65°and in the narrower 2θ range from 5° to 40°. The peaks of TiO_2 in anatase phase from the TNT layer and the peaks for Ti from the underlying Ti substrate are identified. Noticeably, a peak at $2\theta \sim 14.3°$ for MoS_2 is visible [26622-ICSD]. Furthermore, several peaks, marked as Mo_xS_y, can be observed at $2\theta \sim 9.3°$, $2\theta \sim 10.3°$, $2\theta \sim 12.5°$ and $2\theta \sim 13.8°$ stemming from Mo_xS_y with different stoichiometric compositions. The average grain

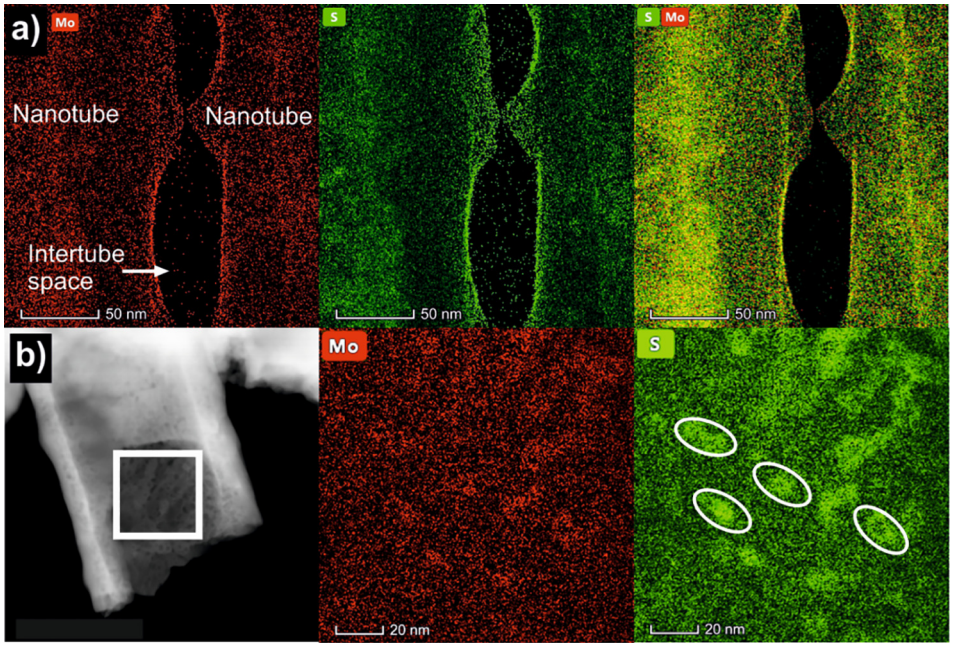

Fig. 2. (a) STEM EDX elemental maps showing distribution of Mo and S species on two adjacent TiO_2 nanotubes and revealing MoS_2 decoration along TNT walls after 2 MoS_2 ALD cycles, and (b) planar view in STEM HAADF image in higher magnification and the STEM EDX elemental maps (corresponding to the region of the marked rectangle) revealing MoS_2 decoration in form of nanosheets on TNT walls after 2 MoS_2 ALD cycles. Ellipses indicate individual nanosheets.

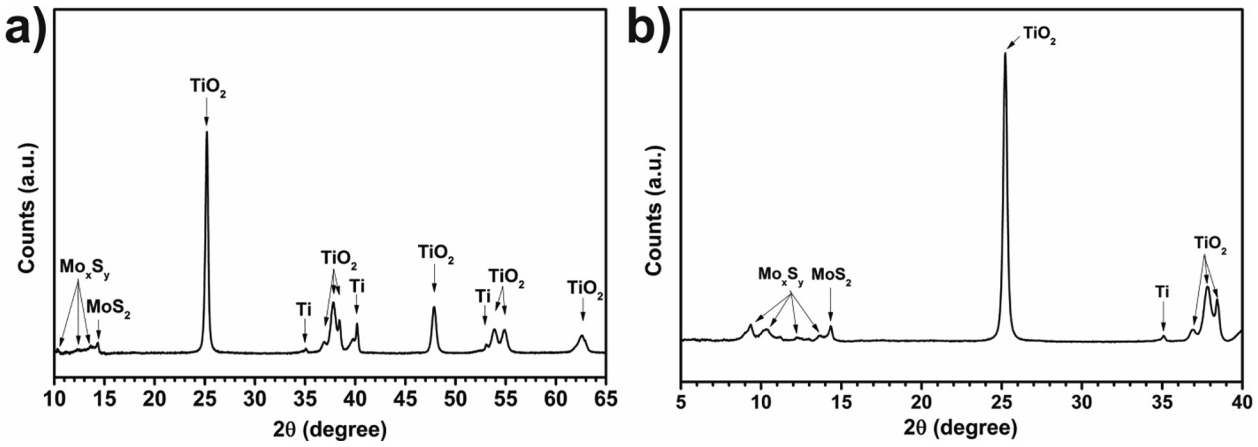

Fig. 3. XRD patterns of the 2 ALD cycles MoS_2 decorated TNT layer. a) full 2θ range scan, b) narrow 2θ range scan.

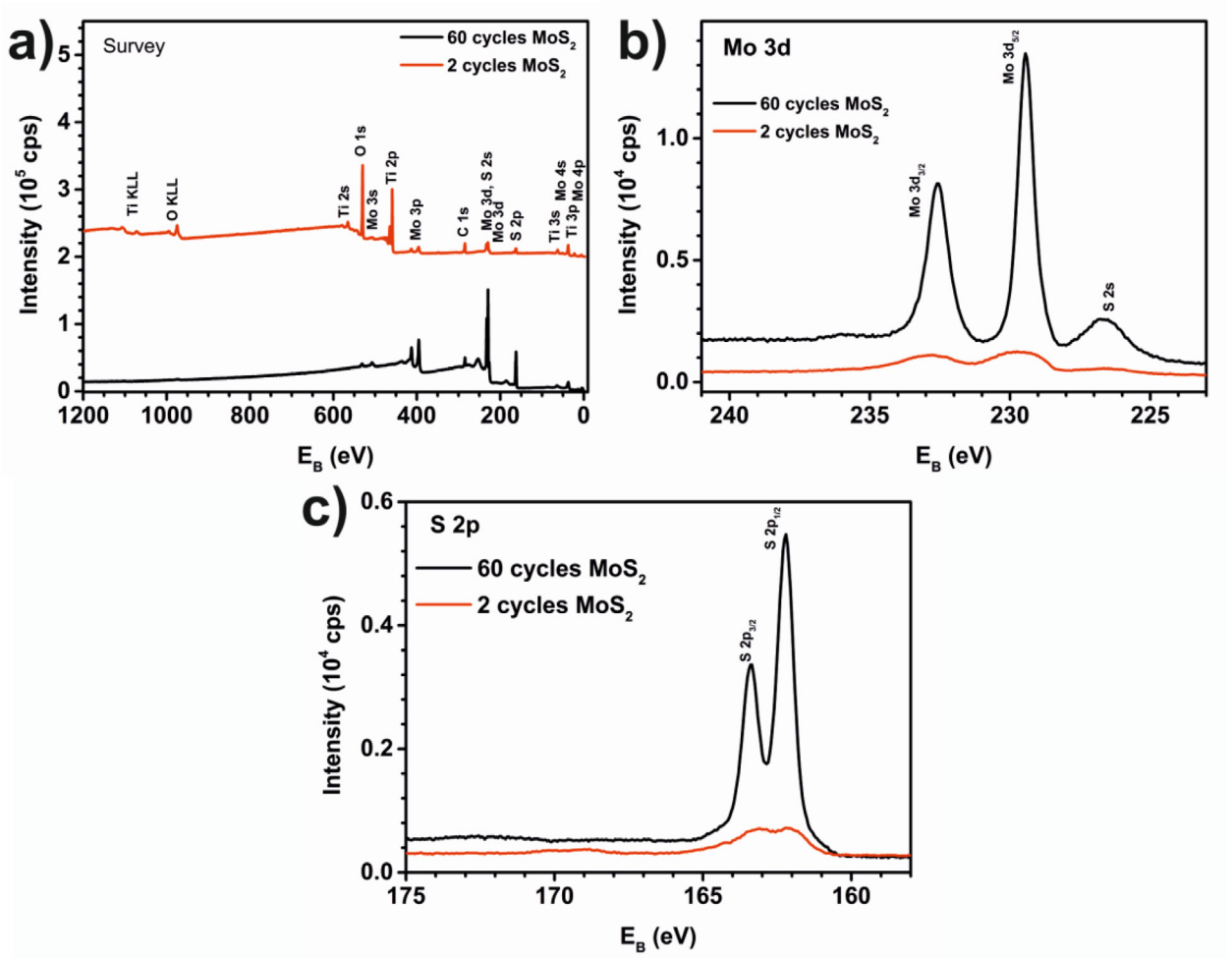

Fig. 4. a) XPS survey spectra, and b) high resolution spectra of Mo 3d and c) high resolution spectra of S 2p for 2 and 60 ALD cycles MoS_2 on a Ti foil.

size of the MoS_2 nanosheets was calculated to be 106 Å using Scherrer equation.

Fig. 4a shows the XPS survey spectra of MoS_2-decorated reference Ti foils (annealed to anatase prior to the ALD decoration), measured in the as-deposited state, while Fig. 4b and c show the high resolution spectra for Mo 3s and S 2p. Because of the higher intensity of the signals of Mo and S as well as lower signals from the underlying Ti substrate, the XPS spectra of Ti foils coated with 60 MoS_2 ALD cycles are additionally shown for reference. For the Ti foils decorated with 2 MoS_2 ALD cycles, Ti and O signals can be observed in the survey scan that stem from the TiO_2 of the underlying annealed Ti foil. The MoS_2 film deposited with 60 ALD cycles is too thick to observe signals from the underlying substrate. The C species detected for both decoration thicknesses can be related to the handling of the samples in air following the ALD process. For the 60 ALD MoS_2 cycles, the high resolution spectra of Mo 3d show a doublet with the Mo $3d_{5/2}$ peak at 229.4 eV corresponding to the Mo^{4+} oxidation state and the spectra of S 2p show a doublet with the S $2p_{1/2}$ peak at 162.2 eV corresponding to the S^{2-} oxidation state. The S

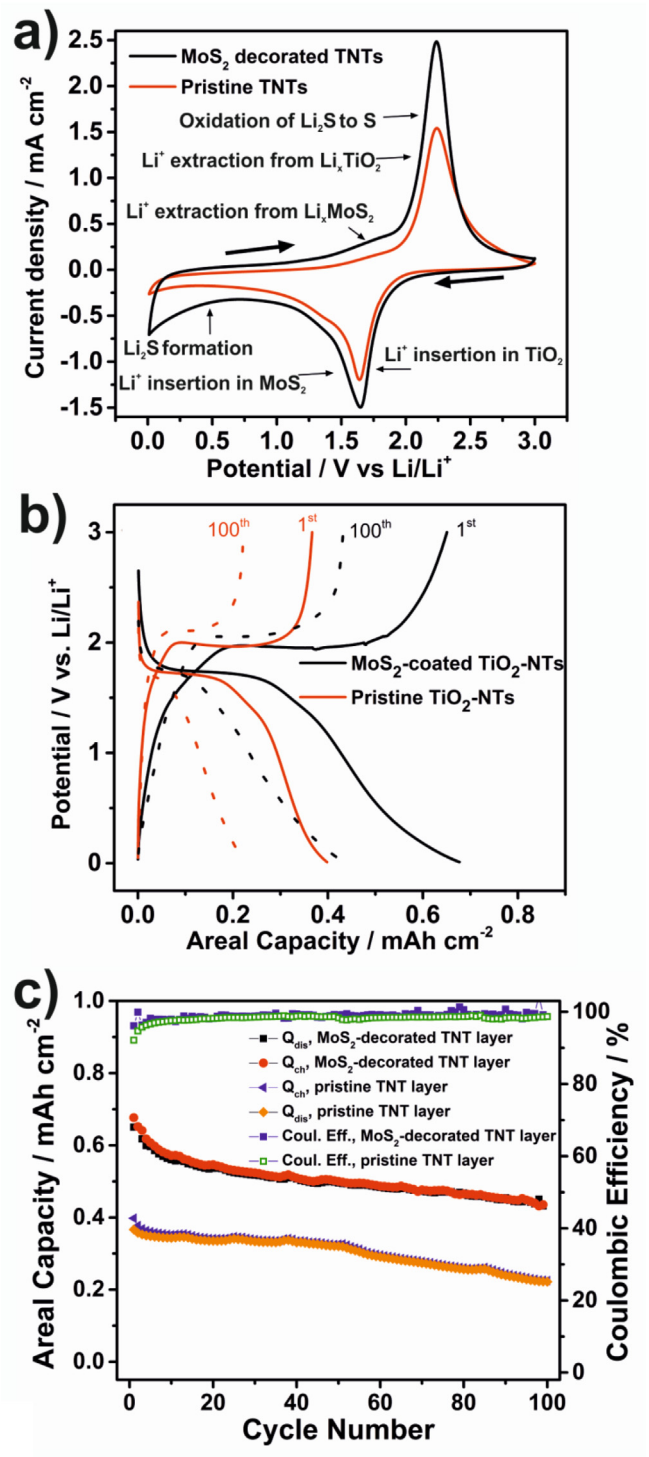

Fig. 5. (a) Cyclic voltammograms of the pristine TNT layer and the MoS_2-decorated TNT layer in the potential range of 0.01–3 V vs Li/Li^+ at a scan rate of 0.5 mV s^{-1}, (b) Galvanostatic charge–discharge profiles and (c) long-term cycle stability performance at 1C rate for the pristine TNT and the MoS_2-decorated TNT layers in the potential range of 0.01–3 V vs Li/Li^+.

to Mo ratio determined from respective spectral areas is 1.95 confirming that the deposited ALD film was MoS_2 [38]. As can be seen in the high resolution spectrum of Mo 3d for the Ti foil decorated with 2 MoS_2 ALD cycles, the doublet shape is wider than that of the sample coated with 60 MoS_2 ALD cycles pointing to the presence of an extra Mo state at the MoS_2 and TiO_2 interface. The S/Mo ratio is found to decrease to 1.75 and might stem from a built up of some Mo-O bonds between the thin TiO_2 thermal oxide layer present on the annealed Ti foil and the MoS_2. When larger sheets of MoS_2 were grown on the Ti foil (e.g. via 60 ALD cycles), the XPS spectrum of Mo 3d exhibits only one dominant doublet state showing pure MoS_2.

3.2. Application of MoS_2-decorated TNTs in μLIBs

Fig. 5a shows the cyclic voltammograms (CV, the first cycle) obtained for the pristine and the MoS_2-decorated (2 ALD cycles) TNT layers. Well-defined cathodic (Li^+ insertion) and anodic (Li^+ extraction) peaks were recorded at 1.68 and 2.2 V vs Li/Li^+, respectively. These peaks correspond to the reversible reaction of Li^+ with anatase TiO_2 according to Eq. (1) [58,65].

$$TiO_2 + xLi^+ + xe^- \leftrightarrow Li_xTiO_2 \quad 0 \le x \le 0.5 \tag{1}$$

Compared to the CV curve of the pristine TNT layer, the MoS_2-decorated TNT layer showed broader peaks and a larger surface area under the CV curve. This effect can be attributed to three main factors. Primarily, it is the result of the multistep reaction of Li^+ with MoS_2. In the cathodic scan, the insertion of Li^+ into MoS_2 to form Li_xMoS_2 occurred in the voltage range of 1.25–1.75 V and further lithiation at 0.3 V led to the formation of Li_2S and Mo according to Eqs. (2) and (3) [30,66,67]. In the reverse anodic scan, the extraction of Li^+ occurred at 1.8 V and 2.3 V corresponding to the retrieve of Li_xMoS_2 and the oxidation of Li_2S to S.

$$MoS_2 + xLi^+ + xe^- \rightarrow Li_xMoS_2 \tag{2}$$

$$Li_xMoS_2 + (4-x)Li^+ + (4-x)e^- \rightleftarrows Mo + 2Li_2S \tag{3}$$

$$Li_2S \rightleftarrows 2Li^+ + 2e^- + S \tag{4}$$

Secondly, the MoS_2-decorated TNT layers possess an increased intrinsic electronic conductivity compared to their blank TNT counterpart. This is clearly seen from the CV curves recorded in aqueous 1 M Na_2SO_4 electrolyte (Fig. S1), where the dark current densities in both, the anodic and cathodic, directions clearly show higher values for the MoS_2-decorated TNT layers. Since the base materials - TNTs layers - are the same, this increased conductivity must stem from the MoS_2 nanosheet decoration. Thirdly, the MoS_2 decoration of TNTs leads to their stabilization in terms of structure and surface chemistry. Previous works on various coatings, such as Al_2O_3, Ag, C, and Co_3O_4, on TNT layers have shown similar effects [8,68–71].

Fig. 5b shows the 1st and 100th galvanostatic charge–discharge profiles obtained at 1C rate for the pristine TNT layer and the MoS_2-decorated TNT layer. The insertion/extraction voltage plateaus were consistent with the redox peaks observed in the CV curves. The first discharge areal capacities for the pristine TNT layer and the MoS_2-decorated TNT layer were attained 0.4 mAh cm^{-2} and 0.67 mAh cm^{-2}, respectively. At the 100th cycle, the areal capacities were equal to 0.22 mAh cm^{-2} for the pristine TNT layer and 0.44 mAh cm^{-2} for the MoS_2-decorated TNT layer. Clearly, a superior capacity was obtained for the MoS_2-coated TNT layer compared to the pristine counterpart. This improvement can be attributed to the additional contribution of ultrathin MoS_2 nanosheets deposited onto a nanotubular support showing a very large surface area. Fig. 5c shows the cycle life performance at 1C for 100 cycles and the corresponding Coulombic efficiencies. The capacity loss observed during cycling occurs probably due to several reasons: the irreversible reaction of Li^+ with trace water molecules, the Li^+ trapping within the structural defects of TiO_2, the dissolution of S, and the formation of a passive layer due to the electrolyte decomposition, the so-called solid electrolyte interphase (SEI) [69,72]. An overall capacity retention of 65% was achieved for the MoS_2-decorated TNT layer, while the pristine TNT layer had an overall capacity retention of 55%. However, even though it is clear that in general higher capacities were obtained in other studies on MoS_2 materials for LIBs [27,28,30,31,67], a remarkable increase of the capacity compared to the pristine TNT layers was obtained by a decoration with ultra-thin

MoS_2 nanosheets, using only 2 MoS_2 ALD cycles. It must be noted that 1 MoS_2 ALD cycles did not lead to a capacity improvement, while higher ALD cycles led to a significant capacity increase upon galvanostatic cycling, however, with a low long-term cycle stability performance. It is, thus, a challenge for future work to optimize the MoS_2 coating thickness and the stability, but the positive prospects are very high.

The Coulombic efficiency (CE) for the MoS_2-decorated TNT layer at the first cycle was 96% and reached more than 98% starting from the second cycle. In comparison, the CE of the pristine TNT layer was 92% and reached 98% after fifteen cycles. The superior CE performance for the coated sample can be attributed to the enhanced electrical conductivity as the result of the MoS_2 coating.

Post-cycling SEM analysis of the pristine and the MoS_2-decorated TNT layers are shown in Fig. S2a and b. As one can see, the nanotubular structure is preserved on both samples after 100 cycles Li insertion/extraction at 1C rate. A thin SEI formation can be observed on the top of the TNT and a somewhat thicker SEI formation was seen in case of the MoS_2-decorated TNT layer. It is known from the literature that the SEI layer built on TiO_2 itself during Li insertion/extraction is very thin [73]. Therefore, a thicker SEI layer can be expected on MoS_2-decorated TNT layers.

Fig. S2c shows the post-cycling XRD patterns for both types of TNT layers. In accordance with the reactions discussed above, $LiMoS_2$ and LiS_2 were observed for the MoS_2-decorated TNT layer. In addition, $Li_xTi_yO_z$ with different stoichiometric composition was observed for the pristine TNT layer. MoS_2 was present in the lithiated form.

A Ragone plot is shown in Fig. S3, comparing the performance of the electrodes used herein (pristine and MoS_2-decorated TNT layers) at 1C with published microbatteries having 3D electrodes. It is clearly shown that the electrochemical performance obtained by MoS_2-decorated TNTs is superior compared to the cells with other 3D electrodes.

4. Conclusions

In conclusion, for the first time the homogenous decoration of high aspect ratio TNT layers with a large density of ultra-thin MoS_2 nanosheets using ALD was shown and a new precursor combination for thermal ALD was introduced. STEM/EDX measurements proved the homogeneous distribution of the MoS_2 nanosheets along the nanotube walls over the whole thickness of the TNT layers. The stoichiometric composition of the MoS_2 nanosheets was confirmed by XPS. Furthermore, the ALD MoS_2-decorated TNT layers were successfully employed as anodes for μLIBs. They clearly reveal a superior electrochemical performance compared to their pristine counterparts.

Declaration of Competing Interest

The authors declare that they have no known competing financial interests or personal relationships that could have appeared to influence the work reported in this paper.

Acknowledgement

The European Research Council (project nr. 638857) and the Ministry of Youth, Education and Sports of the Czech Republic (projects nr. CZ.02.1.01/0.0/0.0/16_013/0001829, LM2015082, LQ1601) are acknowledged for financial support of this work, whose part was carried out with the support of CEITEC Nano Research Infrastructure. TD is grateful to IMT and the Saint-Etienne School of Mines.

Appendix A. Supplementary data

CV curves recorded in an aqueous electrolyte, post-cycling SEM and XRD analysis, Ragone plot. Supplementary data to this article can be found online at https://doi.org/10.1016/j.flatc.2019.100130.

References

[1] J.M. Macak, H. Tsuchiya, A. Ghicov, K. Yasuda, R. Hahn, S. Bauer, P. Schmuki, TiO_2 nanotubes: self-organized electrochemical formation, properties and applications, Curr. Opin. Solid State Mater. Sci. 11 (2007) 3–18, https://doi.org/10.1016/j.cossms.2007.08.004.

[2] P. Roy, S. Berger, P. Schmuki, TiO_2 nanotubes: synthesis and applications, Angew. Chemie Int. Ed. 50 (2011) 2904–2939, https://doi.org/10.1002/anie.201001374.

[3] K. Lee, A. Mazare, P. Schmuki, One-dimensional titanium dioxide nanomaterials: nanotubes, Chem. Rev. 114 (2014) 9385–9454, https://doi.org/10.1021/cr500061m.

[4] I. Paramasivam, J.M. Macak, P. Schmuki, Photocatalytic activity of TiO_2 nanotube layers loaded with Ag and Au nanoparticles, Electrochem. Commun. 10 (2008) 71–75, https://doi.org/10.1016/j.elecom.2007.11.001.

[5] J.M. Macak, B.G. Gong, M. Hueppe, P. Schmuki, Filling of TiO_2 nanotubes by self-doping and electrodeposition, Adv. Mater. 19 (2007) 3027–3031, https://doi.org/10.1002/adma.200602549.

[6] S. Das, H. Sopha, M. Krbal, R. Zazpe, V. Podzemna, J. Prikryl, J.M. Macak, Electrochemical infilling of $CuInSe_2$ within TiO_2 nanotube layers and subsequent photoelectrochemical studies, ChemElectroChem. 4 (2017) 495–499, https://doi.org/10.1002/celc.201600763.

[7] R. Zazpe, H. Sopha, J. Prikryl, M. Krbal, J. Mistrik, F. Dvorak, L. Hromadko, J.M. Macak, A 1D conical nanotubular TiO_2/CdS heterostructure with superior photon-to-electron conversion, Nanoscale 10 (2018) 16601–16612, https://doi.org/10.1039/C8NR02418A.

[8] H. Sopha, G.D. Salian, R. Zazpe, J. Prikryl, L. Hromadko, T. Djenizian, J.M. Macak, ALD Al_2O_3-coated TiO_2 nanotube layers as anodes for lithium-ion batteries, ACS Omega 2 (2017) 2749–2756, https://doi.org/10.1021/acsomega.7b00463.

[9] J.E. Yoo, K. Lee, M. Altomare, E. Selli, P. Schmuki, Self-organized arrays of single-metal catalyst particles in TiO_2 cavities: a highly efficient photocatalytic system, Angew. Chemie Int. Ed. 52 (2013) 7514–7517, https://doi.org/10.1002/anie.201302525.

[10] X. Zhou, M. Lickleder, P. Schmuki, Thin MoS_2 on TiO_2 nanotube layers: an efficient co-catalyst/harvesting system for photocatalytic H_2 evolution, Electrochem. Commun. 73 (2016) 33–37, https://doi.org/10.1016/j.elecom.2016.10.008.

[11] W.-T. Sun, Y. Yu, P. Hua-Yong, X.-F. Gao, Q. Chen, L.-M. Peng, CdS quantum dots sensitized TiO_2 photoelectrodes, J. Am. Chem. Soc. 130 (2008) 1124–1125 https://linkinghub.elsevier.com/retrieve/pii/S0254058409003216.

[12] D.R. Baker, P.V. Kamat, Photosensitization of TiO_2 nanostructures with CdS quantum dots: particulate versus Tubular Support Architectures, Adv. Funct. Mater. 19 (2009) 805–811, https://doi.org/10.1002/adfm.200801173.

[13] J.M. Macak, T. Kohoutek, L. Wang, R. Beranek, Fast and robust infiltration of functional material inside titania nanotube layers: case study of a chalcogenide glass sensitizer, Nanoscale 5 (2013) 9541–9545, https://doi.org/10.1039/c3nr03014h.

[14] S.H. Ju, S. Han, J.S. Kim, The growth and morphology of copper phthalocyanine on TiO_2 nanotube arrays, J. Ind. Eng. Chem. 19 (2013) 272–278, https://doi.org/10.1016/j.jiec.2012.08.011.

[15] L. Guo, Z. Yang, K. Marcus, Z. Li, B. Luo, L. Zhou, X. Wang, Y. Du, Y. Yang, MoS_2/TiO_2 heterostructures as nonmetal plasmonic photocatalysts for highly efficient hydrogen evolution, Energy Environ. Sci. 11 (2018) 106–114, https://doi.org/10.1039/C7EE02464A.

[16] J. Tupala, M. Kemell, E. Härkönen, M. Ritala, M. Leskelä, Preparation of regularly structured nanotubular TiO_2 thin films on ITO and their modification with thin ALD-grown layers, Nanotechnology 23 (2012) 125707, , https://doi.org/10.1088/0957-4484/23/12/125707.

[17] I. Turkevych, S. Kosar, Y. Pihosh, K. Mawatari, T. Kitamori, J. Ye, K. Shimamura, Synergistic effect between TiO_2 and ubiquitous metal oxides on photocatalytic activity of composite nanostructures, J. Ceram. Soc. Jpn. 122 (2014) 393–397, https://doi.org/10.2109/jcersj2.122.P6-1.

[18] F. Dvorak, R. Zazpe, M. Krbal, H. Sopha, J. Prikryl, S. Ng, L. Hromadko, F. Bures, J.M. Macak, One-dimensional anodic TiO_2 nanotubes coated by atomic layer deposition: towards advanced applications, Appl. Mater. Today 14 (2019) 1–20.

[19] B.G. Silbernagel, Lithium intercalation complexes of layerd transition metal dichalcogenides: an NMR survey of physical properties, Solid State Commun. 17 (1975) 361–365.

[20] C.A. Papageorgopoulos, W. Jaegermann, Li intercalation across and along the van der Waals surfaces of MoS_2(0001), Surf. Sci. 338 (1995) 83–93, https://doi.org/10.1016/0039-6028(95)00544-7.

[21] S. Choi, K.C. Kwon, S.Y. Kim, H.W. Jang, Tailoring catalytic activities of transition metal disulfides for water splitting, FlatChem. 4 (2017) 68–80, https://doi.org/10.1016/j.flatc.2017.06.010.

[22] J. Luxa, V. Mazanek, D. Bousa, D. Sedmidubsky, M. Pumera, Z. Sofer, Graphene-amorphous transition-metal chalcogenide (MoSx, WSx) composites as highly efficient hybrid electrocatalysts for the hydrogen evolution reaction, ChemElectroChem. 3 (2016) 565–571 https://onlinelibrary.wiley.com/doi/abs/10.1002/celc.201500497.

[23] M.S. Whittingham, F.R.J. Gamble, The lithium intercalates of the transition metal dichalcogenides, Mater. Res. Bull. 10 (1975) 363–372.

[24] X. Xu, W. Liu, Y. Kim, J. Cho, Nanostructured transition metal sulfides for lithium ion batteries: progress and challenges, Nano Today 9 (2014) 604–630, https://doi.org/10.1016/j.nantod.2014.09.005.

[25] W. Rüdorff, H.H. Sick, Einlagerungsverbindungen von Alkali- und Erdalkalimetallen in Molybdän- und Wolframdisulfid, Angew. Chemie. 71 (1959) 127.

[26] T. Stephenson, Z. Li, B. Olsen, D. Mitlin, Lithium ion battery applications of molybdenum disulfide (MoS_2) nanocomposites, Energy Environ. Sci. 7 (2014) 209–231, https://doi.org/10.1039/C3EE42591F.

[27] C. Feng, J. Ma, H. Li, R. Zeng, Z. Guo, H. Liu, Synthesis of molybdenum disulfide (MoS_2) for lithium ion battery applications, Mater. Res. Bull. 44 (2009) 1811–1815, https://doi.org/10.1016/j.materresbull.2009.05.018.

[28] Y. Teng, H. Zhao, Z. Zhang, Z. Li, Q. Xia, Y. Zhang, L. Zhao, X. Du, Z. Du, P. Lv, K. Świerczek, MoS_2 Nanosheets vertically grown on graphene sheets for lithium-ion battery anodes, ACS Nano 10 (2016) 8526–8535, https://doi.org/10.1021/acsnano.6b03683.

[29] H. Wang, H. Jiang, Y. Hu, Z. Deng, C. Li, Interface engineering of few-layered MoS_2 nanosheets with ultrafine TiO_2 nanoparticles for ultrastable Li-ion batteries, Chem. Eng. J. 345 (2018) 320–326, https://doi.org/10.1016/j.cej.2018.03.166.

[30] C.-Y. Wu, W.-E. Chang, Y.-G. Sun, J.-M. Wu, J.-G. Duh, Three-dimensional S-MoS_2@α-Fe_2O_3 nanoparticles composites as lithium-ion battery anodes for enhanced electrochemical performance, Mater. Chem. Phys. 219 (2018) 311–317, https://doi.org/10.1016/j.matchemphys.2018.08.059.

[31] J.-G. Wang, H. Liu, R. Zhou, X. Liu, B. Wei, Onion-like nanospheres organized by carbon encapsulated few-layer MoS_2 nanosheets with enhanced lithium storage performance, J. Power Sources 413 (2019) 327–333, https://doi.org/10.1016/j.jpowsour.2018.12.055.

[32] G. Liu, J. Cui, R. Luo, Y. Liu, X. Huang, N. Wu, X. Jin, H. Chen, S. Tang, J.-K. Kim, X. Liu, 2D MoS_2 grown on biomass-based hollow carbon fibers for energy storage, Appl. Surf. Sci. 469 (2019) 854–863, https://doi.org/10.1016/j.apsusc.2018.11.067.

[33] T.T. Shan, S. Xin, Y. You, H.P. Cong, S.H. Yu, A. Manthiram, Combining nitrogen-doped graphene sheets and MoS_2: a unique film–foam–film structure for enhanced lithium storage, Angew. Chem. – Int. Ed. 55 (2016) 12783–12788, https://doi.org/10.1002/anie.201606870.

[34] C. Zhao, J. Kong, X. Yao, X. Tang, Y. Dong, S.L. Phua, X. Lu, Thin MoS_2 nanoflakes encapsulated in carbon nanofibers as high-performance anodes for lithium-ion batteries, ACS Appl. Mater. Interfaces 6 (2014) 6392–6398, https://doi.org/10.1021/am4058088.

[35] Z. Zhang, S. Wu, J. Cheng, W. Zhang, MoS_2 nanobelts with (002) plane edges-enriched flat surfaces for high-rate sodium and lithium storage, Energy Storage Mater. 15 (2018) 65–74, https://doi.org/10.1016/j.ensm.2018.03.013.

[36] J. Xiao, D. Choi, L. Cosimbescu, P. Koech, J. Liu, J.P. Lemmon, Exfoliated MoS_2 nanocomposite as an anode material for lithium ion batteries, Chem. Mater. 22 (2010) 4522–4524, https://doi.org/10.1021/cm101254j.

[37] L. Yang, S. Wang, J. Mao, J. Deng, Q. Gao, Y. Tang, O.G. Schmidt, Hierarchical MoS_2/polyaniline nanowires with excellent electrochemical performance for lithium-ion batteries, Adv. Mater. 25 (2013) 1180–1184, https://doi.org/10.1002/adma.201203999.

[38] D.K. Nandi, U.K. Sen, D. Choudhury, S. Mitra, S.K. Sarkar, Atomic layer deposited MoS_2 as a carbon and binder free anode in Li-ion battery, Electrochim. Acta 146 (2014) 706–713, https://doi.org/10.1016/j.electacta.2014.09.077.

[39] M.B. Sreedhara, S. Gope, B. Vishal, R. Datta, A.J. Bhattacharyya, C.N.R. Rao, Atomic layer deposition of crystalline epitaxial MoS_2 nanowall networks exhibiting superior performance in thin-film rechargeable Na-ion batteries, J. Mater. Chem. A 6 (2018) 2302–2310, https://doi.org/10.1039/C7TA09399C.

[40] Z. Jin, S. Shin, D.H. Kwon, S.-J. Han, Y.-S. Min, Novel chemical route for atomic layer deposition of MoS_2 thin film on SiO_2/Si substrate, Nanoscale 6 (2014) 14453–14458, https://doi.org/10.1039/C4NR04816D.

[41] L.K. Tan, B. Liu, J.H. Teng, S. Guo, H.Y. Low, K.P. Loh, Atomic layer deposition of a MoS_2 film, Nanoscale 6 (2014) 10584–10588, https://doi.org/10.1039/C4NR02451F.

[42] J.J. Pyeon, S.H. Kim, D.S. Jeong, S.-H. Baek, C.-Y. Kang, J.-S. Kim, S.K. Kim, Wafer-scale growth of MoS_2 thin films by atomic layer deposition, Nanoscale 8 (2016) 10792–10798, https://doi.org/10.1039/C6NR01346E.

[43] M. Mattinen, T. Hatanpää, T. Sarnet, K. Mizohata, K. Meinander, P.J. King, L. Khriachtchev, J. Räisänen, M. Ritala, M. Leskelä, Atomic layer deposition of crystalline MoS_2 thin films: new molybdenum precursor for low-temperature film growth, Adv. Mater. Interfaces 4 (2017) 1700123, https://doi.org/10.1002/admi.201700123.

[44] T. Jurca, M.J. Moody, A. Henning, J.D. Emery, B. Wang, J.M. Tan, T.L. Lohr, L.J. Lauhon, T.J. Marks, Low-temperature atomic layer deposition of MoS_2 films, Angew. Chemie Int. Ed. 56 (2017) 4991–4995, https://doi.org/10.1002/anie.201611838.

[45] X. Zhou, N. Liu, P. Schmuki, Photocatalysis with TiO_2 nanotubes: “colorful” reactivity and designing site-specific photocatalytic centers into TiO_2 nanotubes, ACS Catal. 7 (2017) 3210–3235, https://doi.org/10.1021/acscatal.6b03709.

[46] M. Shirazi, W.M.M. Kessels, A.A. Bol, Initial stage of atomic layer deposition of 2D-MoS_2 on a SiO_2 surface: a DFT study, PCCP 20 (2018) 16861–16875, https://doi.org/10.1039/C8CP00210J.

[47] A.U. Mane, S. Letourneau, D.J. Mandia, J. Liu, J.A. Libera, Y. Lei, Q. Peng, E. Graugnard, J.W. Elam, Atomic layer deposition of molybdenum disulfide films using MoF_6 and H_2S, J. Vac. Sci. Technol. A Vacuum Surf. Film 36 (2018), https://doi.org/10.1116/1.5003423.

[48] M. Chhowalla, H.S. Shin, G. Eda, L.-J. Li, K.P. Loh, H. Zhang, The chemistry of two-dimensional layered transition metal dichalcogenide nanosheets, Nat. Chem. 5 (2013) 263–275, https://doi.org/10.1038/nchem.1589.

[49] B. Hinnemann, P.G. Moses, J. Bonde, K.P. Jørgensen, J.H. Nielsen, S. Horch, I. Chorkendorff, J.K. Nørskov, Biomimetic hydrogen evolution: MoS_2 nanoparticles as catalyst for hydrogen evolution, J. Am. Chem. Soc. 127 (2005) 5308–5309, https://doi.org/10.1021/ja0504690.

[50] Z. He, W. Que, Molybdenum disulfide nanomaterials: structures, properties, synthesis and recent progress on hydrogen evolution reaction, Appl. Mater. Today 3 (2016) 23–56, https://doi.org/10.1016/j.apmt.2016.02.001.

[51] C. Meng, Z. Liu, T. Zhang, J. Zhai, Layered MoS_2 nanoparticles on TiO_2 nanotubes by a photocatalytic strategy for use as high-performance electrocatalysts in hydrogen evolution reactions, Green Chem. 17 (2015) 2764–2768, https://doi.org/10.1039/C5GC00272A.

[52] W. Teng, Y. Wang, H. Huang, X. Li, Y. Tang, Enhanced photoelectrochemical performance of MoS_2 nanobelts-loaded TiO_2 nanotube arrays by photo-assisted electrodeposition, Appl. Surf. Sci. 433 (2017) 507–517.

[53] Y. Tian, Y. Song, M. Dou, J. Ji, F. Wang, Enhanced photo-assistant electrocatalysis of anodization TiO_2 nanotubes via surrounded surface decoration with MoS_2 for hydrogen evolution reaction, Appl. Surf. Sci. 433 (2018) 197–205, https://doi.org/10.1016/j.apsusc.2017.09.259.

[54] P.X. Zhao, Y. Tang, J. Mao, Y.X. Chen, H. Song, J.W. Wang, Y. Song, Y.Q. Liang, X.M. Zhang, One-Dimensional MoS_2-Decorated TiO_2 nanotube gas sensors for efficient alcohol sensing, J. Alloy. Compd. 674 (2016) 252–258, https://doi.org/10.1016/j.jallcom.2016.03.029.

[55] L. Yang, X. Zheng, M. Liu, S. Luo, Y. Luo, G. Li, Fast photoelectro-reduction of Cr^{VI} over MoS_2@TiO_2 nanotubes on Ti wire, J. Hazard. Mater. 329 (2017) 230–240, https://doi.org/10.1016/j.jhazmat.2017.01.045.

[56] S. Wang, B.Y. Guan, L. Yu, X.W.D. Lou, Rational design of three-layered TiO_2@Carbon@MoS_2 hierarchical nanotubes for enhanced lithium storage, Adv. Mater. 29 (2017) 1702724, https://doi.org/10.1002/adma.201702724.

[57] R. Zazpe, M. Knaut, H. Sopha, L. Hromadko, M. Albert, J. Prikryl, V. Gärtnerová, J.W. Bartha, J.M. Macak, Atomic layer deposition for coating of high aspect ratio TiO_2 nanotube layers, Langmuir 32 (2016) 10551–10558, https://doi.org/10.1021/acs.langmuir.6b03119.

[58] A.T. Tesfaye, O. Mashtalir, M. Naguib, M.W. Barsoum, Y. Gogotsi, T. Djenizian, Anodized Ti_3SiC_2 As an anode material for Li-ion microbatteries, ACS Appl. Mater. Interfaces 8 (2016) 16670–16676, https://doi.org/10.1021/acsami.6b03528.

[59] W. Wei, G. Oltean, C.-W. Tai, K. Edström, F. Björefors, L. Nyholm, High energy and power density TiO_2 nanotube electrodes for 3D Li-ion microbatteries, J. Mater. Chem. A 1 (2013) 8160, https://doi.org/10.1039/c3ta11273j.

[60] B. Mendoza-Sánchez, Y. Gogotsi, Synthesis of two-dimensional materials for capacitive energy storage, Adv. Mater. 28 (2016) 6104–6135, https://doi.org/10.1002/adma.201506133.

[61] A.D.R. Pillai, K. Zhang, K. Bollenbach, D. Nminibapiel, W. Cao, H. Baumgart, V.S.K. Chakracadhanula, C. Kübel, V. Kochergin, ALD growth of PbTe and PbSe superlattices for thermoelectric applications, ECS Trans. 58 (2013) 131–139.

[62] L. Liu, Y. Huang, J. Sha, Y. Chen, Layer-controlled precise fabrication of ultrathin MoS_2 films by atomic layer deposition, Nanotechnology 28 (2017) 195605.

[63] R. Zazpe, J. Prikryl, V. Gärtnerova, K. Nechvilova, L. Benes, L. Strizik, A. Jäger, M. Bosund, H. Sopha, J.M. Macak, Atomic layer deposition Al_2O_3 coatings significantly improve thermal, chemical, and mechanical stability of anodic TiO_2 nanotube layers, Langmuir 33 (2017) 3208–3216, https://doi.org/10.1021/acs.langmuir.7b00187.

[64] V.C. Anitha, R. Zazpe, M. Krbal, J. Yoo, H. Sopha, J. Prikryl, G. Cha, S. Slang, P. Schmuki, J.M. Macak, Anodic TiO_2 nanotubes decorated by Pt nanoparticles using ALD: an efficient electrocatalyst for methanol oxidation, J. Catal. 365 (2018) 86–93, https://doi.org/10.1016/j.jcat.2018.06.017.

[65] B.L. Ellis, P. Knauth, T. Djenizian, Three-dimensional self-supported metal oxides for advanced energy storage, Adv. Mater. 26 (2014) 3368–3397, https://doi.org/10.1002/adma.201306126.

[66] B. Lu, J. Liu, R. Hu, H. Wang, J. Liu, M. Zhu, C@MoS_2@PPy sandwich-like nanotube arrays as an ultrastable and high-rate flexible anode for Li/Na-ion batteries, Energy Storage Mater. 14 (2018) 118–128, https://doi.org/10.1016/j.ensm.2018.02.022.

[67] L. Wang, Q. Zhang, J. Zhu, X. Duan, Z. Xu, Y. Liu, H. Yang, B. Lu, Nature of extra capacity in MoS_2 electrodes: molybdenum atoms accommodate with lithium, Energy Storage Mater. 16 (2019) 37–45, https://doi.org/10.1016/j.ensm.2018.04.025.

[68] M.M. Rahman, J.-Z. Wang, D. Wexler, Y.-Y. Zhang, X.-J. Li, S.-L. Chou, H.-K. Liu, Silver-coated TiO_2 nanostructured anode materials for lithium ion batteries, J. Solid State Electrochem. 14 (2010) 571–578, https://doi.org/10.1007/s10008-009-0807-4.

[69] W. Wang, Q. Sa, J. Chen, Y. Wang, H. Jung, Y. Yin, Porous TiO_2/C nanocomposite shells As a high-performance anode material for lithium-ion batteries, ACS Appl. Mater. Interfaces 5 (2013) 6478–6483, https://doi.org/10.1021/am402350n.

[70] M. Madian, A. Eychmüller, L. Giebeler, Current advances in TiO_2-based nanostructure electrodes for high performance lithium ion batteries, Batteries 4 (2018) 7, https://doi.org/10.3390/batteries4010007.

[71] Y. Fan, N. Zhang, L. Zhang, H. Shao, J. Wang, J. Zhang, C. Cao, Co_3O_4-coated TiO_2 nanotube composites synthesized through photo-deposition strategy with enhanced performance for lithium-ion batteries, Electrochim. Acta 94 (2013) 285–293, https://doi.org/10.1016/j.electacta.2013.01.114.

[72] A.T. Tesfaye, Y. Gogotsi, T. Djenizian, Tailoring the morphological properties of anodized Ti_3SiC_2 for better power density of Li-ion microbatteries, Electrochem. Commun. 81 (2017) 29–33, https://doi.org/10.1016/j.elecom.2017.05.010.

[73] T. Djenizian, I. Hanzu, P. Knauth, Nanostructured negative electrodes based on titania for Li-ion microbatteries, J. Mater. Chem. 21 (2011) 9925–9937, https://doi.org/10.1039/c0jm04205f.